PHYSICAL REVIEW D **95,** 075009 (2017)

Constraints on two-Higgs-doublet model parameters in light of rare B decays

Mureed Hussain,[1,*] Muhammad Usman,[1,†] Muhammad Ali Paracha,[1,‡] and Muhammad Jamil Aslam[2,§]

[1]*Department of Physics, School of Natural Sciences (SNS), National University of Sciences and Technology (NUST), Sector H-12, 44000 Islamabad, Pakistan*

[2]*Department of Physics, Quaid-i-Azam University, 45320 Islamabad, Pakistan*

(Received 28 August 2016; revised manuscript received 19 February 2017; published 6 April 2017)

We established the allowed parameters of the two-Higgs-doublet model (2HDM) from flavor physics observables—more precisely, from rare B-meson decays. In our analysis, the most formidable constraints on the 2HDM parameters arise from the branching ratio of rare radiative B-meson decay, i.e. $B \to X_s\gamma$. However, the constraints arising from the branching ratio of $B_s \to \mu^+\mu^-$ decay in the $m_{H^\pm}$ - $\tan\beta$ plane give $m_{H^\pm} > 80$ GeV for the value of $\tan\beta \sim 2$, which is in agreement with large electron-positron collider (LEP) data. Furthermore, we also investigate the bounds on the CP-even m_H and CP-odd m_{A^0} Higgs boson not only from the above mentioned physical observables, but also from the zero crossing of the forward-backward asymmetry of $B \to K^*\mu^+\mu^-$ decay. Therefore, these bounds on parameters of the 2HDM will provide fertile ground to test the 2HDM at current and future B-physics experiments.

DOI: 10.1103/PhysRevD.95.075009

I. INTRODUCTION

The discovery of the Higgs boson by ATLAS and CMS experiments at the Large Hadron Collider (LHC) [1,2] completes the only missing ingredient of the Standard Model (SM). In most cases, the results predicted by the SM are in good agreement with current experimental data, but still there are some unanswered questions that the SM cannot address, such as the hierarchy problem, neutrino masses, dark matter, etc. In order to answer these questions, a number of new physics (NP) models have been proposed in literature. The NP signatures can be investigated through two possible approaches: In the first approach, direct observation, the effects of NP can be probed by smashing the particles at an adequately large energy and then exploring the different particles produced as a result of this collision. The dedicated experiments for this purpose are the ATLAS and the CMS at the LHC. In the second approach, the NP effects can be explored via precision studies, especially in flavor physics, and the devoted experiments for precision frontiers are the LHCb and Belle II at the super-KEKB. The flavor physics processes are among the most suitable candles to explore the NP in the precision approach, especially the rare decays of B and K mesons. The rare B-meson decays are the ideal laboratory system to investigate NP as well as the nonperturbative aspects of QCD at low-energy frontiers. As mentioned earlier, in most of the cases, the predictions of the SM are in consensus with current experimental data, but there are some anomalies at the level of 3σ observed in certain flavor physics observables. For example, the LHCb results on the branching ratio of $B_s \to \phi\mu^+\mu^-$ in the two large-recoil bins deviate at the 3σ level from the SM predictions [3]. Likewise, the LHCb analysis of the 3 fb^{-1} of data on $B \to K^*\mu^+\mu^-$ confirms the anomaly (at the 3σ level) [4] that they have observed in the two large-K^* recoil bins of angular observables P_5' [5,6] during their analysis of 1 fb^{-1} data in 2013 [7]. In addition, a measurement of the ratio of the branching fractions of the $B^+ \to K^+\mu^+\mu^-$ and $B^+ \to K^+e^+e^-$ decays shows a 2.6σ deviation from the SM predictions [8]. To resolve the issues that appear repeatedly in various observables in these decay modes, there exist plenty of NP models, such as models with extra dimensions [9,10], the little Higgs model [11,12], family nonuniversal Z' models [13,14], and the supersymmetric standard model [15]. One of the most popular extensions of the SM is the two-Higgs-doublet model (2HDM) suggested by Lee [16] as a means of explaining the matter-antimatter asymmetry [17,18]. A nice and comprehensive review of the 2HDM was presented in Ref. [18]. Just to be brief here, in the 2HDM, in addition to the SM Higgs doublet, an additional complex Higgs doublet was considered which then leads to two scalars (h, H), one pseudoscalar (A), and two charged $(H^\pm)$ Higgs bosons. The vacuum expectation values (VEVs) of the 2HDM are represented by v_1 and v_2, and the interactions of the fermions with the Higgs field, through which they acquire mass, depend on the tangent of the ratio of the VEV; i.e., $\tan\beta = \frac{v_2}{v_1}$, and it serves as a free parameter in the 2HDM. In general, the 2HDM owns the FCNC transition at tree level, which can be avoided by imposing an *ad hoc* discrete symmetry [19]. Imposing an *ad hoc* symmetry

*mureed.hussain@sns.nust.edu.pk
†muhammadusman@sns.nust.edu.pk
‡aliphoton9@gmail.com
§muhammadjamil.aslam@gmail.com

TABLE I. Relations between the fermion mass matrices and Yukawa coupling matrices in four 2HDM models.

	Type I	Type II	Type III	Type IV
ρ_D	$\kappa^D \cot(\beta)$	$-\kappa^D \tan(\beta)$	$-\kappa^D \tan(\beta)$	$\kappa^D \cot(\beta)$
ρ_U	$\kappa^U \cot(\beta)$	$\kappa^U \cot(\beta)$	$\kappa^U \cot(\beta)$	$\kappa^U \cot(\beta)$
ρ_L	$\kappa^L \cot(\beta)$	$-\kappa^L \tan(\beta)$	$\kappa^L \cot(\beta)$	$-\kappa^L \tan(\beta)$

motivates to two different possibilities in the 2HDM, namely the types I and II. In type I, in order to retain the flavor conservation at tree level, all the fermions couple with one of the Higgs doublet, whereas in the type-II scenario, the 2HDM somehow harmonizes with the minimal supersymmetric model (MSSM); i.e., the up- and down-type quarks couple with two different Higgs doublets, and so they are the charged leptons. In addition to these two types, there are two other versions of the 2HDM in which the down-type quarks and charged leptons acquire mass from different doublets: type III and type IV [20], and all four of these types of 2HDM are summarized in Table I. From the experimental observation of branching ratios of $b \to s\gamma$ and the measurement of the Higgs boson at the LHC [21,22], one can get the indirect constraints on the masses of the 2HDM along with the constraint on $\tan\beta$. This has been done in the past; Hou *et al.* [23] have discussed the charged Higgs boson effects on the loop induced B-meson decays. Also, in some recent studies (cf. Ref. [24]), a lower limit of 304 GeV on the charged Higgs mass in 2HDM type II is established by the branching ratio of $b \to s\gamma$. In Refs. [25,26], constraints from $B_{s,d} \to \mu^+\mu^-$, $B \to \tau\nu$, and $B \to X_s\gamma$ are applied to a charged Higgs boson and $\tan\beta$ in all four types of 2HDM. In the present work, we provide a comprehensive analysis of all types of 2HDM in light of rare B decays. In particular, we implement constraints on scalars, pseudoscalars, charged Higgs boson masses and coupling parameters of the 2HDM from the ALEPH Collaboration results on the branching ratio of $b \to s\gamma$ [27], and from the LHCb Collaboration results on the branching ratio of $B_s \to \mu^+\mu^-$ [28], along with the measurement of the zero crossing of lepton forward-backward asymmetry (A_{FB}) of $B \to K^*\mu^+\mu^-$ [29].

II. THEORETICAL FRAMEWORK

A. Overview of the two-Higgs-doublet model

In line with the SM of particle physics, the 2HDM has the only extension in the Higgs sector where an extra Higgs doublet is introduced, and it leaves all the other particle contents the same. In general, the scalar potential in the 2HDM has 11 independent parameters, but imposing a particular symmetry will reduce the number of free parameters. In most of the 2HDM models, a discrete Z_2 symmetry is imposed which takes the first doublet $\Phi_1 \to \Phi_1$ (Z_2 even) and the second doublet $\Phi_2 \to -\Phi_2$ (Z_2 odd). The implications of Z_2 symmetry leave us with eight free parameters in CP-conserving potential—namely the four masses; the rotation angle in the CP-even sector, α; the ratio of the vacuum expectation values, $\tan\beta = v_2/v_1$; and the soft breaking parameter m_{12}^2—and these, along with their explicit form, are explained in detail in Ref. [30]. Just like the mass generation of fermions in the SM, in the 2HDM the fermions can get mass because of the Yukawa coupling of y_{ij} to the Higgs doublet Φ. In the 2HDM, the Yukawa couplings to the first scalar doublet Φ_1 are fixed, because the interactions have to be diagonal both in flavor space and in mass eigenstate basis. However, in the case of the second scalar doublet Φ_2, the couplings are nondiagonal and cannot be related to fermion masses. The mass eigenstates for fermions can be written as vectors in flavor space; therefore, the 2HDM Yukawa sector can be expressed in terms of physical Higgs mass eigenstates as [31]

$$\begin{aligned}\mathcal{L}_{\text{Yukawa}} = &-\frac{1}{\sqrt{2}}\bar{D}\{\kappa^D \sin(\beta-\alpha) + \rho^D \cos(\beta-\alpha)\}Dh - \frac{1}{\sqrt{2}}\bar{D}\{\kappa^D \cos(\beta-\alpha) - \rho^D \sin(\beta-\alpha)\}DH \\ &- \frac{i}{\sqrt{2}}\bar{D}\gamma_5\rho^D DA - \frac{1}{\sqrt{2}}\bar{U}\{\kappa^U \sin(\beta-\alpha) + \rho^U \cos(\beta-\alpha)\}Uh - \frac{1}{\sqrt{2}}\bar{U}\{\kappa^U \cos(\beta-\alpha) \\ &- \rho^U \sin(\beta-\alpha)\}UH - \frac{i}{\sqrt{2}}\bar{U}\gamma_5\rho^U UA - \frac{1}{\sqrt{2}}\bar{L}\{\kappa^L \sin(\beta-\alpha) + \rho^L \cos(\beta-\alpha)\}Lh \\ &- \frac{1}{\sqrt{2}}\bar{L}\{\kappa^L \cos(\beta-\alpha) - \rho^L \sin(\beta-\alpha)\}LH - \frac{i}{\sqrt{2}}\bar{L}\gamma_5\rho^L LA \\ &- [\bar{U}(V_{CKM}\rho^D P_R - \rho^U V_{CKM}P_L)DH^+ + \bar{\nu}\rho^L P_R LH^+ + \text{H.c.}]. \end{aligned} \quad (1)$$

In Eq. (1), the κ^F's (where $F = U, D, L$) are the 3×3 diagonal matrices with the definition $\kappa^F \equiv \sqrt{2}M^F/v$, where the M^F's are the corresponding fermion mass matrices. The detailed expressions of these matrices are given in Ref. [32]. The Lagrangian given in Eq. (1) has the freedom to choose an arbitrary value of ρ^F. However, the allowed sizes of the off-diagonal elements in ρ^F have stringent constraints, because nonzero elements instigate a

Higgs-mediated FCNC transition at tree level. Just for the sake of completeness, the connections between Yukawa coupling matrices ρ^F and fermion mass matrices κ^F in four different types of 2HDM models [32] are summarized in Table I. The purpose of the present study is to look for the constraints on all physical Higgs masses and coupling parameters in the light of the rare B-meson decays. In the framework of the 2HDM type-III Yukawa interaction, the Cheng-Sher-Yuan (CSY) parametrization [33,34] for the couplings $\varepsilon_{ij} = \frac{m_i m_j}{v^2}\lambda_{ij}$ is useful, and among these, the third-family couplings λ_{bb} and λ_{tt} are constrained, along with the charged Higgs boson mass, from the branching ratios of $b \to s\gamma$ and $B^+ \to l^+\nu$ [35]. They have shown that the most stringent constraints are coming from $b \to s\gamma$, and the pure leptonic decays can only exclude regions with small λ_{bb} and small $m_{H^\pm}$. They have not used semileptonic rare B decays, which we have applied in this article, and we also use updated values of the branching ratios of radiative and pure leptonic B decays. Here, in the given notation of Yukawa couplings $\varepsilon_{ij} = \kappa^F \nu_{ij} + \rho^F \mu_{ij}$,

$$H_a = U_{ab}\Phi_b = \begin{pmatrix} \nu_{11}^* & \nu_{12}^* \\ \mu_{21}^* & \mu_{22}^* \end{pmatrix}\Phi_b = \begin{pmatrix} \nu_{11}^* & \nu_{12}^* \\ -\nu_{12} & \nu_{11} \end{pmatrix}\Phi_b, \tag{2}$$

where ν_{ij} and μ_{ij} relate the Higgs basis H and the generic basis Φ [36].

B. Effective Hamiltonian

The phenomenology of the rare B-meson decays can be studied by using the effective Hamiltonian approach, where one can separate the short-distance physics (encoded in Wilson coefficients) from the long-distance (concealed in transition form factors). The effective Hamiltonian for the rare radiative decay $b \to s\gamma$ and rare semileptonic decays $b \to s\ell^+\ell^-$ ($\ell = e, \mu, \tau$) are given as follows [37]:

$$\mathcal{H}_{\rm eff}(b \to s\gamma) = \frac{4G_F}{\sqrt{2}} \sum_{p=u,c,t} V_{ps}^* V_{pb} \sum_{i=1}^{8} C_i(\mu) O_i(\mu), \tag{3}$$

$$\mathcal{H}_{\rm eff}(b \to s\ell^+\ell^-) = -\frac{4G_F}{\sqrt{2}} V_{tb} V_{ts}^* \left(\sum_{i=1}^{10} C_i(\mu) O_i(\mu) + \sum_{i=1}^{10} C_{Q_i}(\mu) Q_i(\mu) \right). \tag{4}$$

In Eqs. (3) and (4), $O_i(\mu)$ are the four quark local operators, and $C_i(\mu)$ are the corresponding Wilson coefficients which are evaluated at energy scale μ, which for the B-meson decays is the b-quark mass (m_b). The explicit form of the operators responsible for the decays of the B-meson can be summarized as follows [38]:

$$\begin{aligned}
O_1 &= (\bar{s}\gamma_\mu T^a P_L c)(\bar{c}\gamma^\mu T^a P_L b), \qquad O_2 = (\bar{s}\gamma_\mu P_L c)(\bar{c}\gamma^\mu P_L b),\\
O_3 &= (\bar{s}\gamma_\mu P_L b)\sum_q (\bar{q}\gamma^\mu q), \qquad O_4 = (\bar{s}\gamma_\mu T^a P_L b)\sum_q (\bar{q}\gamma^\mu T^a q),\\
O_5 &= (\bar{s}\gamma_\mu\gamma_\nu\gamma_\rho P_L b)\sum_q (\bar{q}\gamma^\mu\gamma^\nu\gamma^\rho q), \qquad O_6 = (\bar{s}\gamma_\mu\gamma_\nu\gamma_\rho T^a P_L b)\sum_q (\bar{q}\gamma^\mu\gamma^\nu\gamma^\rho T^a q),\\
O_7 &= \frac{e}{16\pi^2}[\bar{s}\sigma^{\mu\nu}(m_s P_L + m_b P_R)b]F_{\mu\nu}, \qquad O_8 = \frac{g}{16\pi^2}[\bar{s}\sigma^{\mu\nu}(m_s P_L + m_b P_R)T^a b]G^a_{\mu\nu},\\
O_9 &= \frac{e^2}{(4\pi)^2}(\bar{s}\gamma^\mu b_L)(\bar{\ell}\gamma_\mu \ell), \qquad O_{10} = \frac{e^2}{(4\pi)^2}(\bar{s}\gamma^\mu b_L)(\bar{\ell}\gamma_\mu\gamma_5 \ell),\\
Q_1 &= \frac{e^2}{16\pi^2}(\bar{s}_L^\alpha b_R^\alpha)(\bar{\tau}\tau), \qquad Q_2 = \frac{e^2}{16\pi^2}(\bar{s}_L^\alpha b_R^\alpha)(\bar{\tau}\gamma_5\tau),\\
Q_3 &= \frac{g^2}{16\pi^2}(\bar{s}_L^\alpha b_R^\alpha)\sum_q (\bar{q}_L^\beta q_R^\beta), \qquad Q_4 = \frac{g^2}{16\pi^2}(\bar{s}_L^\alpha b_R^\alpha)\sum_q (\bar{q}_R^\beta q_L^\beta),\\
Q_5 &= \frac{g^2}{16\pi^2}(\bar{s}_L^\alpha b_R^\beta)\sum_q (\bar{q}_L^\beta q_R^\alpha), \qquad Q_6 = \frac{g^2}{16\pi^2}(\bar{s}_L^\alpha b_R^\beta)\sum_q (\bar{q}_R^\beta q_L^\alpha),\\
Q_7 &= \frac{g^2}{16\pi^2}(\bar{s}_L^\alpha \sigma^{\mu\nu} b_R^\alpha)\sum_q (\bar{q}_L^\beta \sigma_{\mu\nu} q_R^\beta), \qquad Q_8 = \frac{g^2}{16\pi^2}(\bar{s}_L^\alpha \sigma^{\mu\nu} b_R^\alpha)\sum_q (\bar{q}_R^\beta \sigma_{\mu\nu} q_L^\beta),\\
Q_9 &= \frac{g^2}{16\pi^2}(\bar{s}_L^\alpha \sigma^{\mu\nu} b_R^\beta)\sum_q (\bar{q}_L^\beta \sigma_{\mu\nu} q_R^\alpha), \qquad Q_{10} = \frac{g^2}{16\pi^2}(\bar{s}_L^\alpha \sigma^{\mu\nu} b_R^\beta)\sum_q (\bar{q}_R^\beta \sigma_{\mu\nu} q_L^\alpha).
\end{aligned} \tag{5}$$

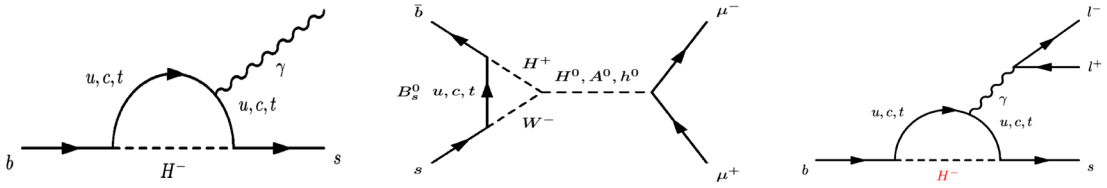

(a) b → s γ (b) $B_s \to \mu^+ \mu^-$ (c) B → $K^*\mu^+\mu-$

FIG. 1. Feynman diagrams of the three important rare decays involving the b quark.

In Eq. (5), the operators $O_i(i = 1, \ldots, 10)$ are in the SM basis, whereas the new operators $Q_i(i = 1, \ldots, 10)$ correspond to the contributions from neutral Higgs boson (NHB) exchange diagrams, and they are depicted in Fig. 1. The explicit form of the Wilson coefficients for NHBs are given below [39]:

$$
\begin{aligned}
C_{Q_1}(m_W) &= \frac{m_b m_\ell}{m_{h^0}^2}\tan^2\beta\frac{1}{\sin^2\theta_W}\frac{x}{4} \\
&\times \left\{(\sin^2\alpha + h\cos^2\alpha) f_1(x,y)\right. \\
&+ \left[\frac{m_{h^0}^2}{m_W^2} + (\sin^2\alpha + h\cos^2\alpha)(1-z)\right] f_2(x,y) \\
&\left. - \frac{\sin^2 2\alpha}{4}\frac{(m_{h^0}^2 - m_{H^0}^2)^2}{m_{h^0}^2 m_{H^0}^2}\right\}, \\
C_{Q_2}(m_W) &= -\frac{m_b m_\ell}{m_{A^0}^2}\tan^2\beta\frac{1}{\sin^2\theta_W}\frac{x}{4} \\
&\times \left\{f_1(x,y) + \left(1 - \frac{m_{H^\pm}^2 - m_{A^0}^2}{m_W^2}\right) f_2(x,y)\right\}, \\
C_{Q_3}(m_W) &= \frac{m_b e^2}{m_\ell g^2}(C_{Q_1}(m_W) + C_{Q_2}(m_W)), \\
C_{Q_4}(m_W) &= \frac{m_b e^2}{m_\ell g^2}(C_{Q_1}(m_W) - C_{Q_2}(m_W)), \\
C_{Q_i}(m_W) &= 0, \qquad i = 5, \ldots, 10,
\end{aligned}
$$

where $x = m_t^2/m_W^2$, $y = m_t^2/m_H^{\pm 2}$, $h = m_h^2/m_H^2$, and $z = x/y$.

III. SCANNING TECHNIQUE FOR 2HDM PARAMETERS AND EXPERIMENTAL CONSTRAINTS FROM RARE *B* DECAYS

In order to study the constraints on the parameters of the 2HDM, we use a two-Higgs-doublet model calculator (2HDMC) which is a C++ code and is based on object-oriented programming [40]. In the 2HDMC package, one has a choice to tune the Higgs potential parameters, and in the Yukawa sector it also gives us the freedom to enumerate the couplings which lead to the FCNC. In this package, standard choices of Yukawa couplings were used, and here types I to IV represent different Yukawa couplings as demonstrated in Table I. The 2HDMC also examines the theoretical properties of the 2HDM, such as the unitarity of the S-matrix and positivity of the potential. As described earlier, in the present study we perform the random scan on the 2HDM physical basis parameters such as $\{m_h, m_H, m_A, m_{H^\pm}, m_{12}^2, \tan\beta, \sin(\beta-\alpha), \lambda_6, \lambda_7;\}$ in the following range:

$$
\begin{aligned}
124.0 \le m_h &\le 126.0 \text{ (GeV)}, \\
0 \le m_H &\le 1000 \text{ (GeV)}, \\
0 \le m_A &\le 1000 \text{ (GeV)}, \\
0 \le m_{H^\pm} &\le 1000 \text{ (GeV)}, \\
-5000 \le m_{12}^2 &\le 5000 \text{ (GeV)}, \\
0 \le \tan\beta &\le 10, \\
-1 \le \sin(\beta-\alpha) &\le 1,
\end{aligned} \tag{6}
$$

where m_h is the SM-like Higgs boson, while m_H, m_A, and $m_{H^\pm}$ are the CP-even, CP-odd, and charged Higgs bosons, respectively. m_{12}^2 is a free parameter in the Yukawa Lagrangian of the 2HDM as defined in Ref. [32], and $\tan\beta$ is the ratio of the vacuum expectation values of the two Higgs doublets. Making use of the Z_2 symmetry on the Yukawa Lagrangian, we set $\lambda_6 = \lambda_7 = 0$. As mentioned above, our goal is to investigate the 2HDM parameters in light of rare B decays; for this purpose we embed 2HDMC on SuperIso v3.4 [41] to study the flavor physics observables such as the branching ratios of $b \to s\gamma$, $B_s \to \mu^+\mu^-$ and the zero crossing of the forward-backward asymmetry of $B \to K^*\mu^+\mu^-$. We then use values of these observables to constrain the 2HDM parameter space. The following experimental values of $\mathrm{BR}(B \to X_s\gamma)$, $\mathrm{BR}(B_s \to \mu^+\mu^-)$, and the zero crossing q_0^2 of the forward-backward asymmetry A_{FB} of $B \to K^*\mu^+\mu^-$ are used to constrain the 2HDM parameters:

$$
\begin{aligned}
\mathrm{BR}(B \to X_s\gamma) &= (3.36 \pm 0.23) \times 10^{-4}, \\
\mathrm{BR}(B_s \to \mu^+\mu^-) &= 3.0^{+1.0}_{-0.9} \times 10^{-9}, \\
q_0^2 &= 4.9 \pm 0.9.
\end{aligned} \tag{7}
$$

IV. RESULTS AND ANALYSIS

In this section, we present the scan over the 2HDM parameter space given in Eq. (6). In all figures, the gray region is consistent with the unitarity of the S-matrix

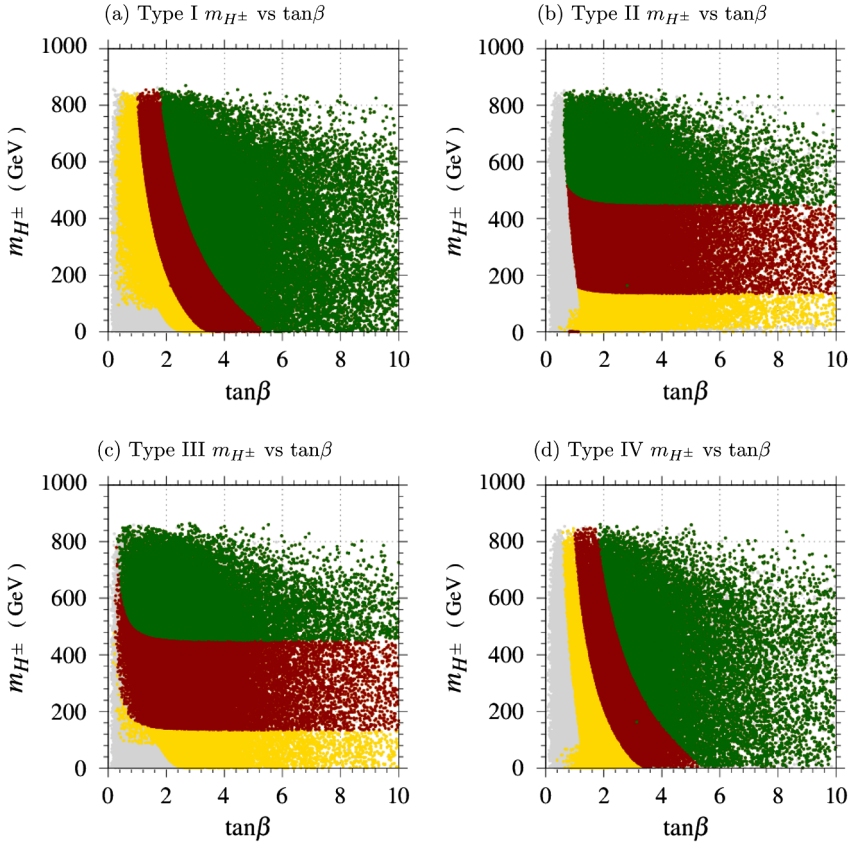

FIG. 2. The effects of constraints on the $\tan\beta$ vs $m_{H^\pm}$ plane that stem from the branching ratio of $B \to \mu^+\mu^-$, the zero crossing (q_0^2) of forward-backward asymmetry of $B \to K^*\mu^+\mu^-$, and the branching ratio of $b \to s\gamma$ are shown in yellow, red, and green shading, respectively.

and the positivity of the potential of the 2HDM. The yellow region is the subset of the gray region that satisfies the constraint from BR($B_s \to \mu^+\mu^-$), whereas the red region is the subset of the yellow region that satisfies the constraints from the zero position of A_{FB} in $B \to K^*\mu^+\mu^-$. The green region is the subset of the red region that satisfies the constraint from BR($B \to X_s\gamma$). Figure 2 shows the effect of the above mentioned decays on the $m_{H^\pm}$-$\tan\beta$ plane of the 2HDM. The most stringent constraints in all types of 2HDM arise from $b \to s\gamma$ decay. The second most important constraint is from A_{FB} of $B \to K^*\mu^+\mu^-$, whereas the effects of $B_s \to \mu^+\mu^-$ on $m_{H^\pm}$-$\tan\beta$ in all 2HDM planes are minimal. In general, the upper limit on $m_{H^\pm}$ in 2HDM is 840 GeV (cf. Fig. 2). Figure 2(a) represents type I of the 2HDM. In this figure, one can see that for low values of $\tan\beta$ ($\tan\beta \sim 2$), the value of $m_{H^\pm}$ should be greater than 80 GeV, which is consistent with the LEP data [42] and also with the value of $m_{H^\pm}$ that is constrained from BR($B_s \to \mu^+\mu^-$). From the zero crossing of A_{FB} of $B \to K^*\mu^+\mu^-$, the allowed value is $\tan\beta > 2.5$, but this value of $\tan\beta$ reduces to 1 when we increase $m_{H^\pm}$ to 800 GeV. The constraints from BR($B \to X_s\gamma$) imply that $\tan\beta \leq 4.5$ is not allowed for $m_{H^\pm} \sim 80$ GeV, but this lower bound also decreases when we increase $m_{H^\pm}$, and for $m_{H^\pm} \sim 800$ GeV the value of $\tan\beta \sim 2.0$.

In Fig. 2(b), we present type II of the 2HDM, in which $\tan\beta \leq 1$ is not allowed for all above mentioned constraints. We can see from this figure that $m_{H^\pm} < 125$ GeV is not allowed from the constraint of the zero crossing of A_{FB}. However, things get more interesting from the constraints of the branching ratio of the decay $B \to X_s\gamma$, as in this case, the lower limit of $m_{H^\pm} \sim 460$ GeV, and so the allowed band for $m_{H^\pm}$ narrows (460 GeV $\leq m_{H^\pm} \leq$ 840 GeV). This is in accordance with the bounds given on $m_{H^\pm}$ by doing NNLO calculations for $B \to X_s\gamma$ decay by Misiak *et al.* [43]. In Fig. 2(c), we discuss type III of the 2HDM, in which the effects of constraints on $m_{H^\pm}$ are similar to those of type II. The only difference is for $m_{H^\pm} < 85$ GeV, which anyhow is not allowed by LEP. Similarly, most of the limits on these two parameters in type IV of the 2HDM are in accordance with those of type I. The possible differences are only for $\tan\beta < 1$ and $m_{H^\pm} < 85$ GeV, which in any case are out of the possible allowed region. The similarity in the above results is due to the fact that for pure leptonic decay, the Yukawa coupling ρ_L is the same for types I and III, so the trends of constraints from the branching ratio of $B_s \to \mu^+\mu^-$ are the same for these two types. Likewise, the Yukawa coupling ρ_L is the same in types II and IV. In contrast to this, the Yukawa coupling ρ_D is the same in types I and IV, and likewise for

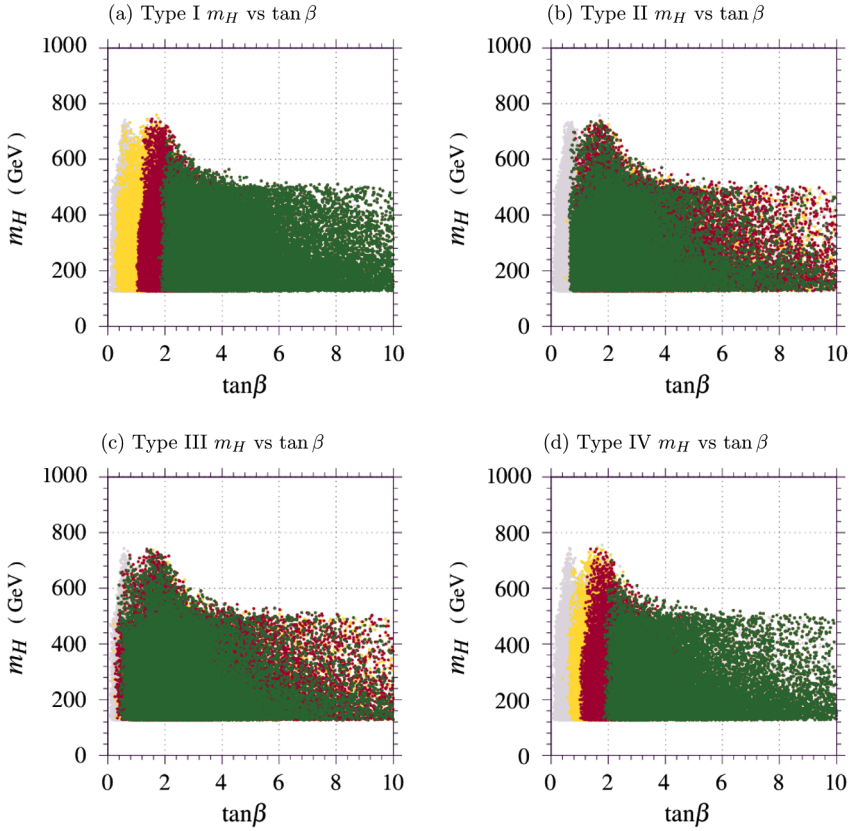

FIG. 3. The effects of constraints on the m_H vs $\tan\beta$ plane. Color coding is the same as in Fig. 2.

type-II and type-III versions of 2HDM. Therefore, the constraints from the zero crossing of A_{FB} and from the branching ratio of $B \to X_s\gamma$ are same for type I and type IV, while they are similar for type II and type III. In Fig. 3, we display our results in the m_H-$\tan\beta$ plane. From these plots, one can see that while increasing the value of $\tan\beta$, the upper limit of m_H decreases. To be precise, for the value of $\tan\beta \sim 6$, m_H cannot be higher than 500 GeV. We also infer the effects of constraints from the above mentioned rare B-meson decays which are similar in types I and IV of 2HDM, whereas these constraints have no effect on types II and III. Also, from Figs. 3(a) and 3(d), the value of $\tan\beta \leq 1$ is not allowed due to the constraints of the zero crossing of A_{FB}, and similar to this, $\tan\beta \leq 2$ is forbidden by the constraints of $\mathrm{BR}(B \to X_s\gamma)$ decay. In Fig. 4, we show the behavior of a pseudoscalar Higgs boson (m_{A^0}) with $\tan\beta$. As long as the mass of the pseudoscalar Higgs is concerned, one can notice that almost all the mass range of m_{A° is allowed in the type-I and type-III versions of the 2HDM. But at the same time, we can see that $\tan\beta < 2$ is not allowed in type I [cf. Fig. 4(a)]. From Fig. 4(b), the lower bound on m_{A° can be predicted to be 60 GeV and 120 GeV from the constraints of the zero crossing of A_{FB} and $\mathrm{BR}(B \to X_s\gamma)$, respectively.

Now, let us discuss the behavior of coupling λ_{tt} with the mass of the charged Higgs boson $(m_{H^\pm})$ in all four types of the 2HDM. As we have already mentioned, the most stringent constraints on the masses of the 2HDM parameters stem from $\mathrm{BR}(B \to X_s\gamma)$, and the least stringent constraint is coming from $\mathrm{BR}(B_s \to \mu^+\mu^-)$. This trend persists for the couplings λ_{tt} and $|\lambda_{bb}|$. In Fig. 5(a), it can be observed that the constraints on λ_{tt} from the branching ratio $B_s \to \mu^+\,\mu^-$ allow almost all values of λ_{tt}. However, things change when we constrain these two parameters from the other two observables. For example, one can see that the allowed range of λ_{tt}, from the constraint coming from the zero crossing of A_{FB}, linearly increases from 0.3 to 1 as we increase $m_{H^\pm}$. From the constraints of $\mathrm{BR}(B \to X_s\gamma)$, the allowed range for coupling λ_{tt} is more restricted, and the upper limit is 0.55 when $m_{H^\pm} \approx 800$ GeV. At 80 GeV, the range of the allowed values of λ_{tt} increases linearly, with the maximum value of 1.55 at $m_{H^\pm} \approx 800$ GeV. In Fig. 5(c), we can see that the constraints on $m_{H^\pm}$ are similar to those of type II. Likewise, the trend of λ_{tt} and $m_{H^\pm}$ is similar to type I in the type-IV version of the 2HDM [cf. Fig. 5(d)].

Another interesting thing is to look for the allowed region of λ_{tt} when it is plotted against the mass of the CP-even neutral Higgs boson (m_H) in all four Yukawa types of the 2HDM. In the case of types I and IV of the 2HDM, as depicted in Figs. 6(a) and 6(d), respectively, for $m_H \leq 500$ GeV, the value of λ_{tt} cannot be greater then 1 when constrained by the zero crossing of A_{FB}. Also, we can see that $\lambda_{tt} > 0.5$ is not allowed from constraints

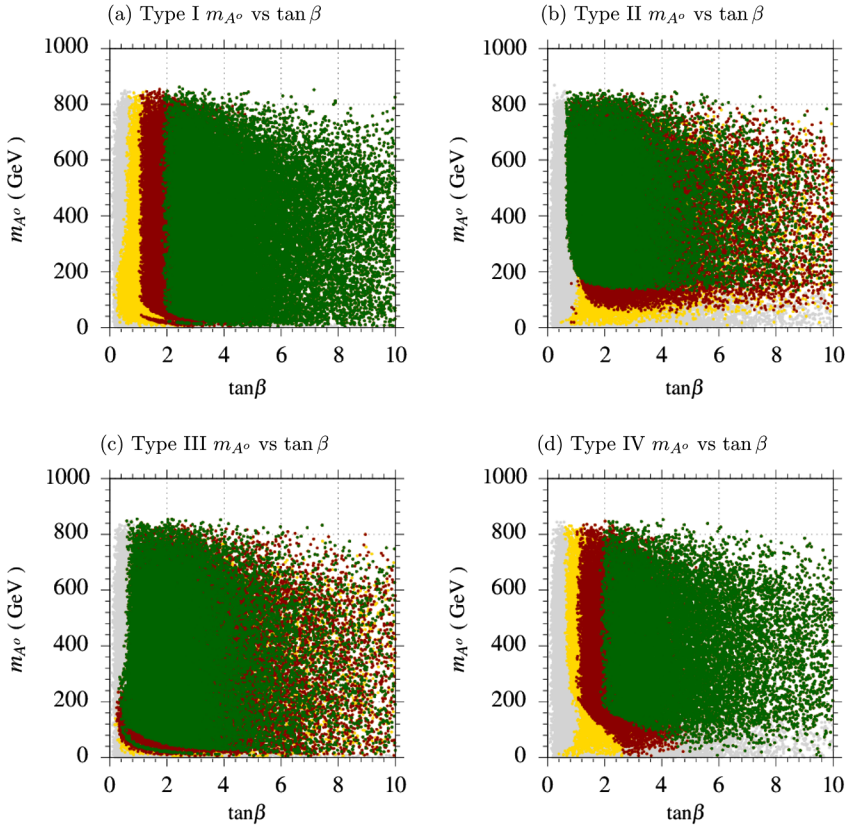

FIG. 4. The effects of constraints on the m_{A^o} vs $\tan\beta$ plane. Color coding is the same as in Fig. 2.

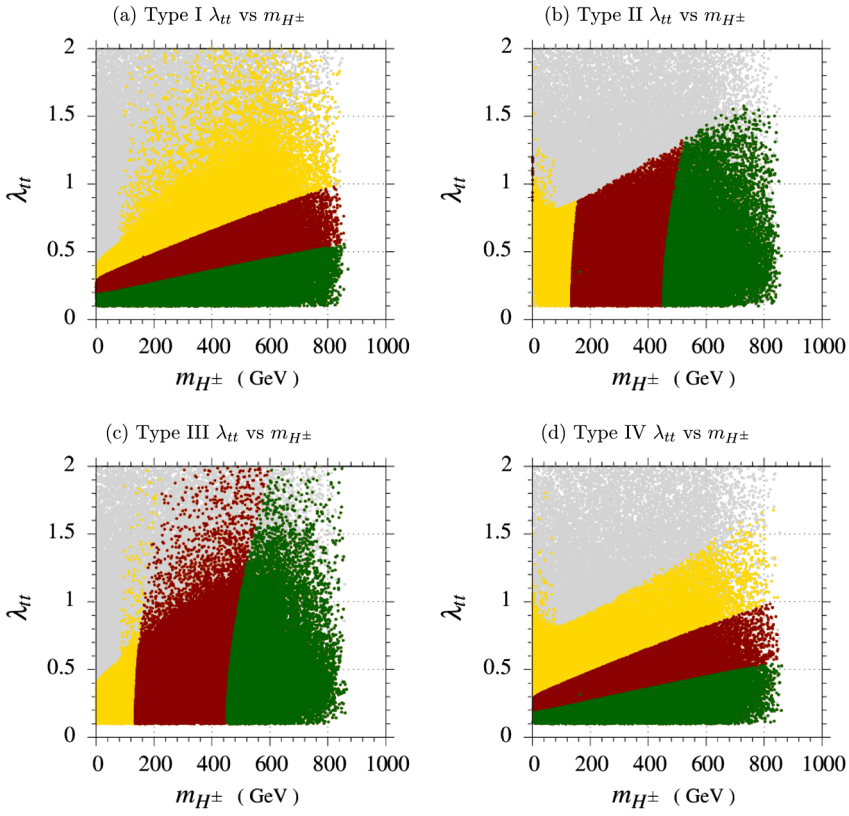

FIG. 5. The effects of constraints on the λ_{tt} vs $m_{H^\pm}$ plane. Color coding is the same as in Fig. 2.

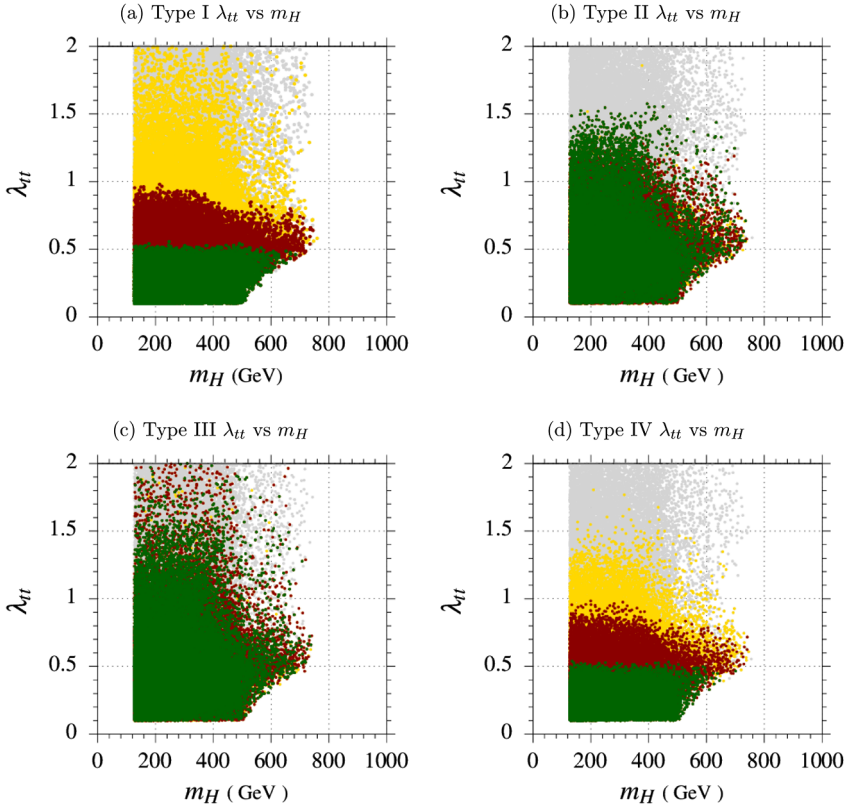

FIG. 6. The effects of constraints on the λ_{tt} vs m_H plane. Color coding is the same as in Fig. 2.

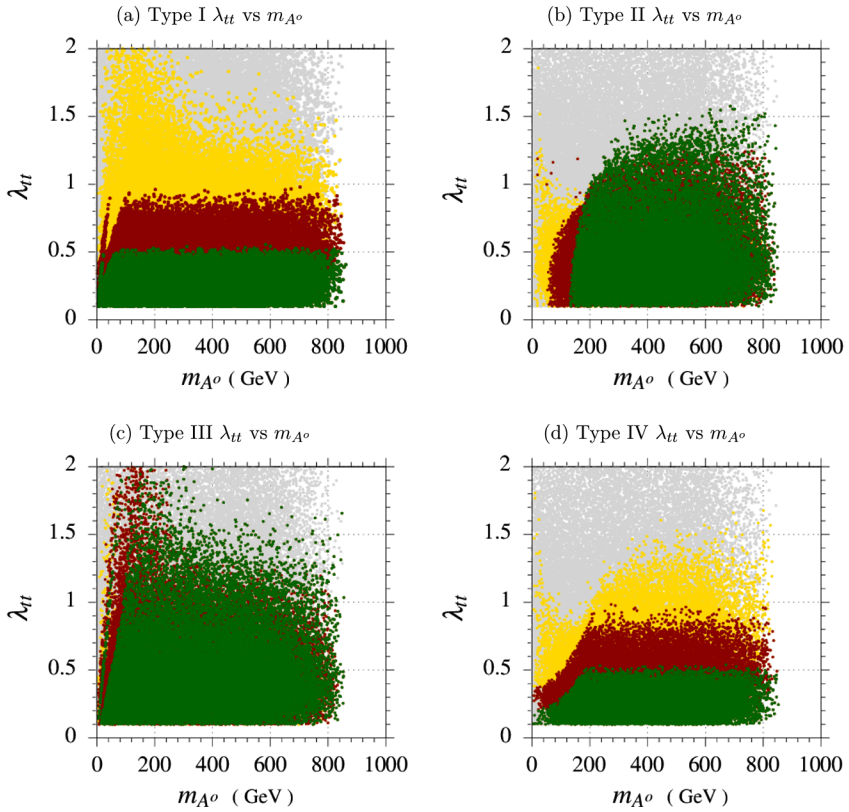

FIG. 7. The effects of constraints on the λ_{tt} vs m_{A^o} plane. Color coding is the same as in Fig. 2.

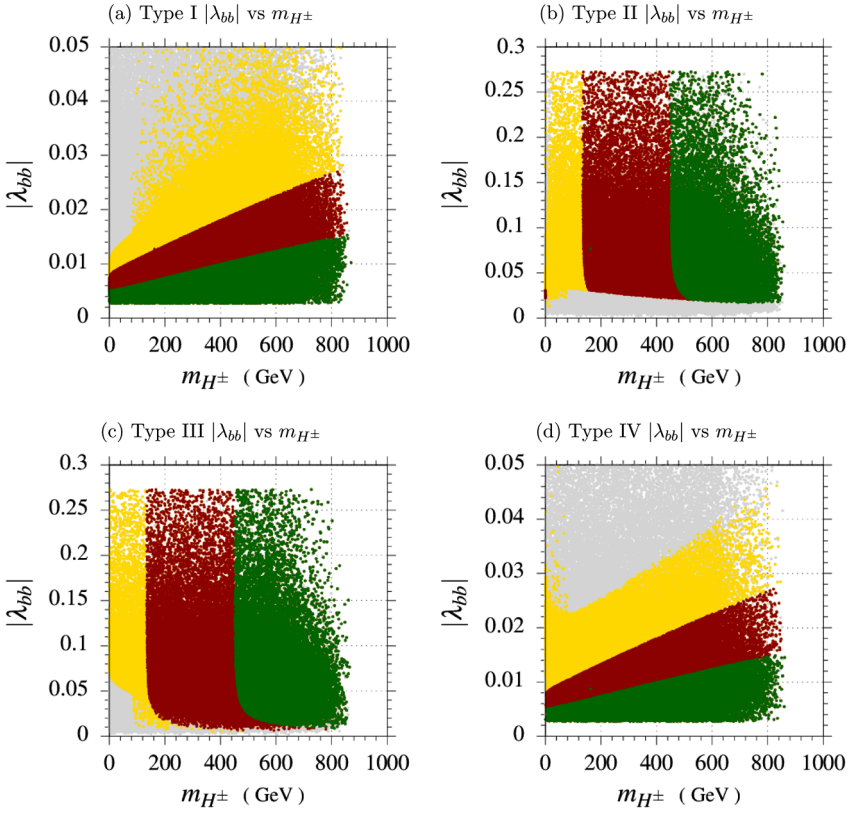

FIG. 8. The effects of constraints on the $|\lambda_{bb}|$ vs $m_{H^\pm}$ plane. Color coding is the same as in Fig. 2.

arising due to BR$(B \to X_s\gamma)$. On the other hand, in the case of types II and III of the 2HDM, as displayed in Figs. 6(b) and 6(c), respectively, there is no constraint on these parameters from the input B-meson decays. Also, for higher values of m_H (i.e., for $m_H \simeq 700$ GeV), $\lambda_{tt} < 0.5$ is not allowed in any of the four types of the 2HDM. In Fig. 7, we display the variation of λ_{tt} with the mass of a pseudoscalar Higgs boson (m_{A°). In the case of types I and IV, the constraints on λ_{tt} from q_0^2 and $b \to s\gamma$ are similar. For example, taking into account the constraints from q_0^2, for $m_{A^\circ} < 200$ GeV, there is a linear increase in the λ_{tt} up to $\lambda_{tt} \simeq 1$; and for $m_{A^\circ} > 200$ GeV, λ_{tt} can attain values up to 1. Likewise, from $b \to s\gamma$, for $m_{A^\circ} \leq 160$ GeV, there is again a linear (almost) increase in the allowed range of λ_{tt} that can go to $\lambda_{tt} \simeq 0.5$ in this mass range. However, for the rest of the mass range, λ_{tt} can have any value less than 0.5. Now, from $B_s \to \mu^+\mu^-$, by looking at the trend of λ_{tt}, it can be noticed that this decay does not give any particular effects in the case of type I of the 2HDM. For type IV, the allowed range of λ_{tt} increases as we increase m_{A°, but the upper limit for λ_{tt} for this type is $\lambda_{tt} \simeq 1.75$. However, for type II of the 2HDM, in Fig. 7(b), λ_{tt} cannot be greater than 1.6; whereas for type III, as plotted in Fig. 7(c), there is no bound on λ_{tt} for $m_{A^\circ} \leq 400$ GeV, and for $m_{A^\circ} > 400$ GeV, λ_{tt} should be less than 1.75.

The constraints on $|\lambda_{bb}|$ with $m_{H^\pm}$ from the above mentioned B-meson decays are plotted in Fig. 8. In Fig. 8(a), we can observe that from $B_s \to \mu^+\mu^-$ decay, in the case when $m_{H^\pm} > 85$ GeV, the entire range of $|\lambda_{bb}| \simeq 0.05$ is allowed. However, when we bring in q_0^2, there is a linear increase in the allowed range of $|\lambda_{bb}|$ as we increase $m_{H^\pm}$. One can see that $|\lambda_{bb}| \simeq 0.028$ is the maximum possible value for $m_{H^\pm} \simeq 800$ GeV. Similarly, when we try to apply constraints from $b \to s\gamma$ decay, again the trend of $|\lambda_{bb}|$ is linearly increasing, and $|\lambda_{bb}| \simeq 0.016$ for $m_{H^\pm} \simeq 800$ GeV. Now, for type II of the 2HDM, in Fig. 8(b), the upper bound on $|\lambda_{bb}|$ is $|\lambda_{bb}| \simeq 0.27$. The same is the case for type III, as can be seen in Fig. 8(c). In case of type IV, shown in Fig. 8(d), the constraints from q_0^2 and $b \to s\gamma$ are similar to those in Fig. 8(a). But when the constraints from $B_s \to \mu^+\mu^-$ are applied, there is also a linear increase in the allowed range of $|\lambda_{bb}|$ for the relative increment in $m_{H^\pm} > 85$ GeV, and the maximum possible value is $|\lambda_{bb}| \simeq 0.046$.

We next show our results in the $|\lambda_{bb}|$-m_H plane in Fig. 9. In the case of types II and III of the 2HDM [cf. Figs. 9(b) and 9(c), respectively], the upper bound on $|\lambda_{bb}|$ is $|\lambda_{bb}| \simeq 0.27$ for $m_H \simeq 550$ GeV. However, for $m_H > 550$ GeV, this allowed range decreases very sharply, and for the highest allowed value of m_H in our analysis (i.e., $m_H \simeq 750$ GeV), $|\lambda_{bb}| = 0.05$ is fixed. There is a slightly lower bound on $|\lambda_{bb}|$

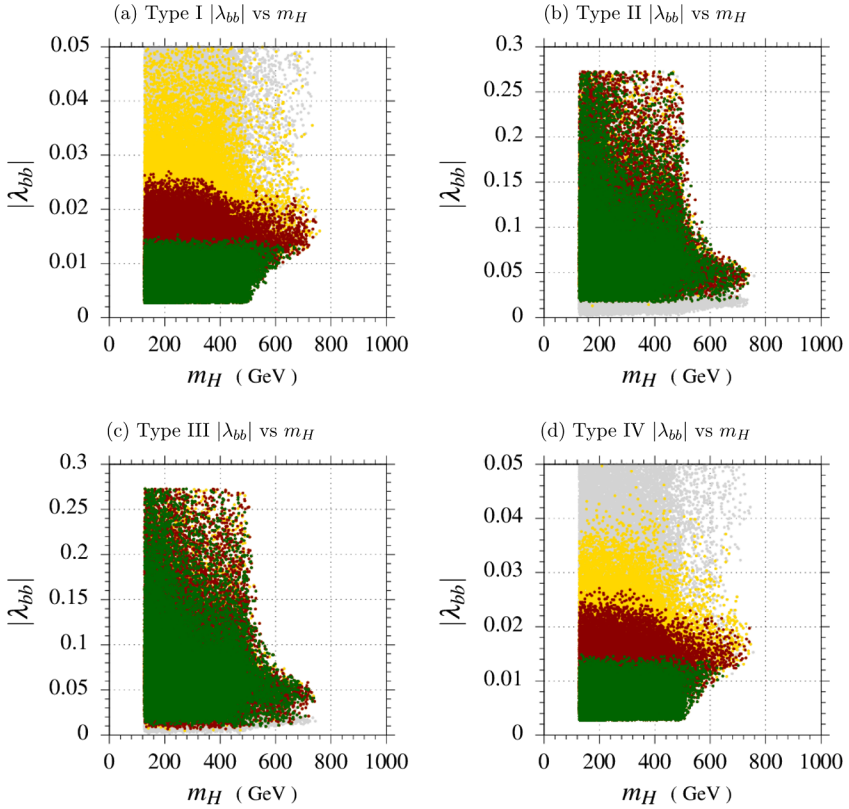

FIG. 9. The effects of constraints on the $|\lambda_{bb}|$ vs m_H plane. Color coding is the same as in Fig. 2.

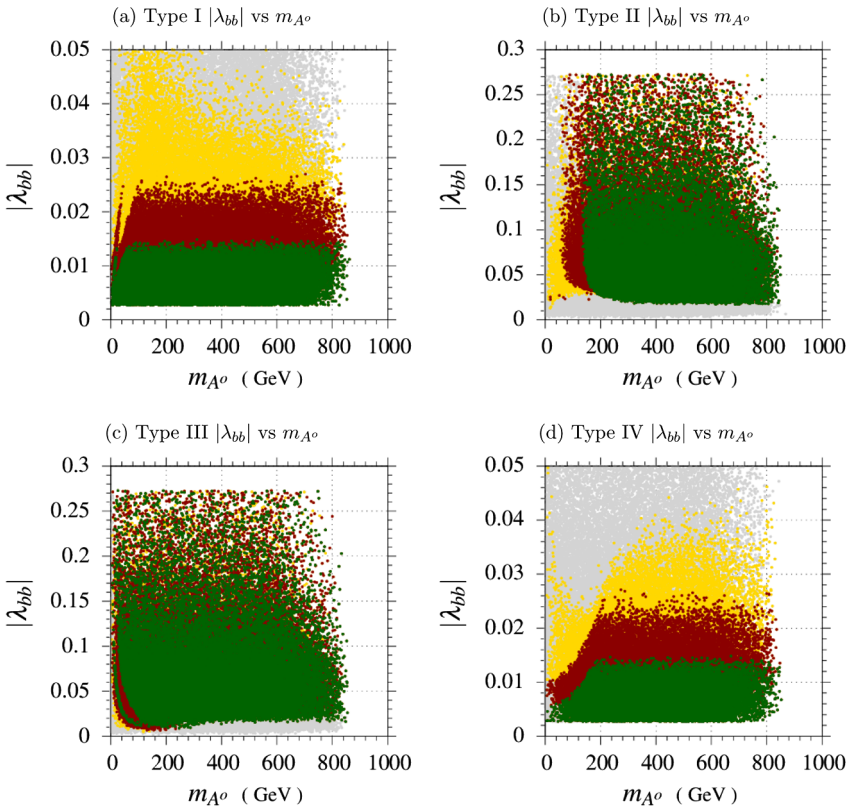

FIG. 10. The effects of constraints on the $|\lambda_{bb}|$ vs m_{A^o} plane. Color coding is the same as in Fig. 2.

for these two types, as for type II $|\lambda_{bb}| \simeq 0.02$, and for type III $|\lambda_{bb}| \simeq 0.01$. In the case of types I and IV of the 2HDM, the trends of B-physics observables are similar. $B_s \to \mu^+\mu^-$ has a very marginal effect on these plots. However, q_0^2 allows $|\lambda_{bb}| \simeq 0.026$ for $m_H \leq 400$ GeV, and this limit slightly decreases to $|\lambda_{bb}| \simeq 0.024$ for $400 < m_H < 500$ GeV. For $m_H > 500$ GeV, the allowed range of $|\lambda_{bb}|$ increases linearly up to $|\lambda_{bb}| \simeq 0.024$.

We next present our results in the $|\lambda_{bb}|$-m_{A^0} plane for the four types of the 2HDM in Fig. 10. In Fig. 10(a), one can notice that $B_s \to \mu^+\mu^-$ has no notable constraint on this plot, whereas q_0^2 allows $|\lambda_{bb}| \leq 0.026$ for the mass range of $m_{A^0} > 80$ GeV. In the case of putting constraints on $|\lambda_{bb}|$ from $B \to X_s\gamma$, the allowed range is $|\lambda_{bb}| \leq 0.014$. Figures 10(b) and 10(c) display the $|\lambda_{bb}|$-m_{A° plane for types II and III of the 2HDM. The upper limit on $|\lambda_{bb}|$ is $|\lambda_{bb}| \simeq 0.27$, which is 10 times higher than the allowed limit for $|\lambda_{bb}|$ in type I by q_0^2 and almost 19 times higher than the allowed limit of $|\lambda_{bb}|$ by $b \to s\gamma$. There is also some difference in the humps, which corresponds to the lower limit on $|\lambda_{bb}|$, between type-II and type-III planes for $m_{A^\circ} \leq 350$ GeV. In the case of type IV, Fig. 10(d), constraints from q_0^2 and $b \to s\gamma$ have similar effects to those of type I in Fig. 10(a). For $B_s \to \mu^+\mu^-$, the trends are different for $m_{A^\circ} \leq 400$ GeV.

V. CONCLUSIONS

In this work, we scanned the parametric space of all four types of the 2HDM by imposing Z_2 symmetry on the Yukawa Lagrangian and by incorporating the experimental constraints from the different observables of rare B-meson decays. In addition to these conditions, the theoretical constraints from the unitarity of the S-matrix and positivity of the potential of 2HDM are also incorporated. The observables which were taken into account to constrain the 2HDM parameters are the branching ratios of $B_s \to X_s\gamma$, $B_s \to \mu^+\mu^-$ and the zero crossing of the forward-backward asymmetry in $B \to K^*\mu^+\mu^-$ decay. Among these three observables, the most stringent constraints come from the branching ratio of $B_s \to X_s\gamma$ that is studied at two loops theoretically in Ref. [43]. The main outcomes of our study can be summarized as follows:

(1) It is observed that for all types of the 2HDM, the upper limit of a charged Higgs boson $m_{H^\pm} \sim 840$ GeV. For type I of the 2HDM in the $m_{H^\pm}$-$\tan\beta$ plane, it is found from the experimental value of the branching ratio of the decay $B_s \to \mu^+\mu^-$ that the lower bound of $m_{H^\pm} > 80$ GeV and is in agreement with LEP data [42] for $\tan\beta \sim 2$. However, for type II of 2HDM, in the same plane, it is found from the experimental value of $B_s \to X_s\gamma$ that the allowed range of $m_{H^\pm}$ is $460 \leq m_{H^\pm} \leq 840$ GeV, and this bound agrees with the theoretical calculations done by Misiak *et al.* [43].

(2) For the CP-even Higgs boson mass m_H, the upper limit is 500 GeV, and for the CP-odd Higgs boson mass m_{A^0}, the upper bound is 840 GeV in all four types of the 2HDM. In the case of the CP-even Higgs boson mass, it is observed that as the value of $\tan\beta$ increases, the upper bound on m_H decreases.

(3) From our analysis of the λ_{tt}-$m_{H^\pm}$, λ_{tt}-m_H, and λ_{tt}-m_{A^0} planes, it can be observed that there are severe bounds on λ_{tt} from the radiative decay of the B meson, and its value cannot be greater than 1 for types I and IV of the 2HDM. However, for type II of the 2HDM, the upper bound on λ_{tt} is 1.55; but for type III, there are no constraints on the upper bounds of λ_{tt}.

(4) From our results for $|\lambda_{bb}|$, we infer that the upper bound on $|\lambda_{bb}|$ is 0.015 from the branching ratio of the decay $B \to X_s\gamma$ for types I and IV of the 2HDM. Furthermore, the upper bound on $|\lambda_{bb}|$ in types II and III of the 2HDM is 0.27—that is, an order of magnitude larger than it is for types I and IV of the 2HDM.

In our analysis, we used the current data of LHCb for the branching ratios of radiative and leptonic decays of B mesons and the zero crossing of forward-backward asymmetry for the decay $B \to K^*\mu^+\mu^-$ to predict the allowed ranges of 2HDM parameters. We hope that the findings of the present study can be tested in future data from LHC.

ACKNOWLEDGMENTS

The authors would like to thank the Research Centre for Modeling and Simulations (RCMS) at the National University of Sciences and Technology (NUST), Islamabad, Pakistan, for providing their supercomputing facility in calculating the results used in this article. M. U. is supported by the National University of Sciences and Technology (NUST), Sector H-12 Islamabad 44000, Pakistan, and the Higher Education Commission (HEC) of Pakistan under Project No. NRPU-3053.

[1] S. Chatrchyan *et al.*, Observation of a new boson at a mass of 125 GeV with the CMS experiment at the LHC, Phys. Lett. B **716**, 30 (2012).

[2] G. Aad *et al.*, Observation of a new particle in the search for the Standard Model Higgs boson with the ATLAS detector at the LHC, Phys. Lett. B **716**, 1 (2012).

[3] R. Aaij *et al.*, Differential branching fraction and angular analysis of the decay $B_s^0 \to \phi\mu^+\mu^-$, J. High Energy Phys. 07 (2013) 084.

[4] R. Aaij *et al.*, Angular analysis of the $B^0 \to K^{*0}\mu^+\mu^-$ decay using 3 fb^{-1} of integrated luminosity, J. High Energy Phys. 02 (2016) 104.

[5] S. Descotes-Genon, J. Matias, M. Ramon, and J. Virto, Implications from clean observables for the binned analysis of $B \to K^*\mu^+\mu^-$ at large recoil, J. High Energy Phys. 01 (2013) 048.

[6] S. Descotes-Genon, T. Hurth, J. Matias, and J. Virto, Optimizing the basis of $B \to K^*\ell\ell$ observables in the full kinematic range, J. High Energy Phys. 05 (2013) 137.

[7] R. Aaij *et al.*, Measurement of Form-Factor-Independent Observables in the Decay $B^0 \to K^{*0}\mu^+\mu^-$, Phys. Rev. Lett. **111**, 191801 (2013).

[8] R. Aaij *et al.*, Test of Lepton Universality Using $B^+ \to K^+\ell^+\ell^-$ Decays, Phys. Rev. Lett. **113**, 151601 (2014).

[9] N. Arkani-Hamed, S. Dimopoulos, and G. R. Dvali, The hierarchy problem and new dimensions at a millimeter, Phys. Lett. B **429**, 263 (1998).

[10] T. Appelquist, H.-C. Cheng, and B. A. Dobrescu, Bounds on universal extra dimensions, Phys. Rev. D **64**, 035002 (2001).

[11] N. Arkani-Hamed, A. G. Cohen, E. Katz, and A. E. Nelson, The littlest Higgs, J. High Energy Phys. 07 (2002) 034.

[12] S. Chang and H.-J. He, Unitarity of little Higgs models signals new physics of UV completion, Phys. Lett. B **586**, 95 (2004).

[13] P. Langacker and M. Plumacher, Flavor changing effects in theories with a heavy Z' boson with family nonuniversal couplings, Phys. Rev. D **62**, 013006 (2000).

[14] V. Barger, L. Everett, J. Jiang, P. Langacker, T. Liu, and C. Wagner, Family nonuniversal $U(1)'$ gauge symmetries and $b \to s$ transitions, Phys. Rev. D **80**, 055008 (2009).

[15] C. Csaki, The minimal supersymmetric standard model (MSSM), Mod. Phys. Lett. A **11**, 599 (1996).

[16] T. D. Lee, A theory of spontaneous T violation, Phys. Rev. D **8**, 1226 (1973).

[17] J. F. Gunion, H. E. Haber, G. L. Kane, and S. Dawson, The Higgs hunter's guide, Front. Phys. **80**, 1 (2000).

[18] G. C. Branco, P. M. Ferreira, L. Lavoura, M. N. Rebelo, M. Sher, and J. P. Silva, Theory and phenomenology of two-Higgs-doublet models, Phys. Rep. **516**, 1 (2012).

[19] S. L. Glashow and S. Weinberg, Natural conservation laws for neutral currents, Phys. Rev. D **15**, 1958 (1977).

[20] V. D. Barger, J. L. Hewett, and R. J. N. Phillips, New constraints on the charged Higgs sector in two Higgs doublet models, Phys. Rev. D **41**, 3421 (1990).

[21] D. Bowser-Chao, K. Cheung, and W.-Y. Keung, Phase effect of a general two Higgs doublet model in $b \to s\gamma$, Phys. Rev. D **59**, 115006 (1999).

[22] B. Dumont, J. F. Gunion, Y. Jiang, and S. Kraml, Constraints on and future prospects for two-Higgs-doublet models in light of the LHC Higgs signal, Phys. Rev. D **90**, 035021 (2014).

[23] W.-S. Hou and R. S. Willey, Effects of extended Higgs sector on loop induced B decays, Nucl. Phys. **B326**, 54 (1989).

[24] O. Deschamps, S. Descotes-Genon, S. Monteil, V. Niess, S. T'Jampens, and V. Tisserand, The two Higgs doublet of type II facing flavour physics data, Phys. Rev. D **82**, 073012 (2010).

[25] X.-D. Cheng, Y.-D. Yang, and X.-B. Yuan, Phenomenological discriminations of the Yukawa interactions in two-Higgs doublet models with Z_2 symmetry, Eur. Phys. J. C **74**, 3081 (2014).

[26] X.-D. Cheng, Y.-D. Yang, and X.-B. Yuan, Revisiting $B_s \to \mu^+\mu^-$ in the two-Higgs doublet models with Z_2 symmetry, Eur. Phys. J. C **76**, 151 (2016).

[27] R. Barate *et al.*, A Measurement of the inclusive $b \to s\gamma$ branching ratio, Phys. Lett. B **429**, 169 (1998).

[28] R. Aaij *et al.*, First Evidence for the Decay $B_s^0 \to \mu^+\mu^-$, Phys. Rev. Lett. **110**, 021801 (2013).

[29] R. Aaij *et al.*, Differential branching fraction and angular analysis of the decay $B^0 \to K^{*0}\mu^+\mu^-$, J. High Energy Phys. 08 (2013) 131.

[30] A. Arhrib, P. M. Ferreira, and R. Santos, Are there hidden scalars in LHC Higgs results?, J. High Energy Phys. 03 (2014) 053.

[31] S. Davidson and H. E. Haber, Basis-independent methods for the two-Higgs-doublet model, Phys. Rev. D **72**, 035004 (2005).

[32] D. Eriksson, J. Rathsman, and O. Stal, 2HDMC: Two-Higgs-Doublet Model Calculator physics and manual, Comput. Phys. Commun. **181**, 189 (2010).

[33] M. Sher and Y. Yuan, Rare B decays, rare τ decays and grand unification, Phys. Rev. D **44**, 1461 (1991).

[34] T. P. Cheng and M. Sher, Mass-matrix ansatz and flavor nonconservation in models with multiple Higgs doublets, Phys. Rev. D **35**, 3484 (1987).

[35] J. P. Idarraga, R. Martinez, J. Alexis Rodriguez, and N. Poveda, Leptonic decays of the B charged meson and $B \to X_{s\gamma}$ in the two Higgs doublet model type III, Braz. J. Phys. **38**, 531 (2008).

[36] H. E. Haber and D. O'Neil, Basis-independent methods for the two-Higgs-doublet model: II. The significance of $\tan\beta$, Phys. Rev. D **74**, 015018 (2006); Erratum, Phys. Rev. D **74**, 059905(E) (2006).

[37] A. J. Buras, Weak Hamiltonian, CP violation and rare decays, in *Probing the Standard Model of Particle Interactions: Proceedings, Summer School in Theoretical Physics, NATO Advanced Study Institute, 68th Session, Les Houches, France, July 28–September 5, 1997*, pp. 281–539.

[38] K. G. Chetyrkin, M. Misiak, and M. Munz, $|\Delta F| = 1$ nonleptonic effective Hamiltonian in a simpler scheme, Nucl. Phys. **B520**, 279 (1998).

[39] Y.-B. Dai, C.-S. Huang, and H.-W. Huang, $B \to X_s \tau^+ \tau^-$ in a two Higgs doublet model, Phys. Lett. B **390**, 257 (1997); Erratum, Phys. Lett. B **513**, 429(E) (2001).

[40] D. Eriksson, J. Rathsman, and O. Stal, 2HDMC: Two-Higgs-doublet model calculator, Comput. Phys. Commun. **181**, 833 (2010).

[41] F. Mahmoudi, SuperIso v2.3: A program for calculating flavor physics observables in Supersymmetry, Comput. Phys. Commun. **180**, 1579 (2009).

[42] K. A. Olive *et al.*, Review of particle physics, Chin. Phys. C **38**, 090001 (2014).

[43] M. Misiak *et al.*, Updated NNLO QCD Predictions for the Weak Radiative B-meson Decays, Phys. Rev. Lett. **114**, 221801 (2015).